CHAPTER IV

SOL–GEL AND SOLID STATE SYNTHESIS AND PROPERTY STUDTY OF

$La_{2-x}Sr_xNiO_4$ $(x \leq 0.8)$

4.1 Abstract

In this study, sol-gel synthesis conditions for the formation of $La_{2-x}Sr_xNiO_4$ (x = 0, 0.2, 0.4, 0.6, and 0.8) compounds were investigated. Effects of Sr substitution on A-site on the properties of the compounds were studied using Fourier transform IR spectroscopy, X-ray diffractometry, scanning electron microscopy, and electrical and thermal analyses. A simple sol-gel preparation process was successfully developed at room temperature using water as the solvent in the presence of ethanolamine as the directing agent. The sol-gel synthesis method was effective in yielding higher purity and more homogenous samples than those synthesized via the solid-state reaction method. The addition of Sr helped stabilize the Ruddlesden-Popper structure, and a highly agglomerated morphology of the sintered samples with Sr substitution was observed, resulting in lower density. Sr helped increase conductivity, whereas its effect on thermal expansion was not as pronounced. $La_{1.2}Sr_{0.8}NiO_4$ synthesized via the sol-gel process provided a conductivity of 160 S/cm at 500°C with a coefficient of thermal expansion value of $13 \times 10^{-6}°C^{-1}$ between 400 and 700°C.

(**Keywords**: Ruddlesden-Popper; Sol-gel process; SOFCs; Cathode)

4.2 Introduction

A major worldwide research thrust in solid oxide fuel cell (SOFC) technology has been the lowering of the system operating temperature from 800-1000 to 400-600°C [1]. The reduction decreases cost, prolongs life, and increases safety of the system, and thus is recognized as a critical step for a successful commercial implementation of SOFCs. Maintaining high efficiency at the lower temperature range has led to a large focus on a new electrode and electrolyte material development. Materials in the group of lanthanum strontium manganite have successfully been used as SOFC cathodes for operation above 800°C. At lower temperatures, however, their conductivities, especially oxygen conductivity, are insufficient [2]. Alternative materials such as lanthanum cobalite perovskites exhibit very good conductivities but exhibit large thermal expansion mismatch with the other cell components, causing thermomechanical failure [3]. Materials with the Ruddlesden-Popper structure (A_2BO_4) such that of the La_2NiO_4 system have been identified as potential cathode materials for the lower operating temperature SOFCs [4]. La_2NiO_4 is also a mixed ionic and electronic conductor with high oxygen diffusivity due to its high oxygen vacancy concentration [5]. Moreover, materials in this group also exhibit coefficient of thermal expansion (CTE) values close to those common SOFC electrolyte materials [6]. The low electronic conductivity of La_2NiO_4, however, needs to be improved [7].

Ishikawa et al. synthesized $LaSrNiO_4$ via solid state using a 1:1 ratio of Sr:La and found that the electron density was almost an order of magnitude larger than that of La_2NiO_4 [8]. Since then, several works on the Sr substitution on the A-site in La_2NiO_4-based system have followed [9-11]. It has been reported that processing route and conditions could strongly affect the properties of the material [4,12,13]. La_2NiO_4 powder is generally synthesized via the solid-state method using oxides, carbonates, or nitrates. Necessarily high firing temperatures result in a low surface area and yield fuel cells with low power because of limited exchange current density. More recently, polymeric methods such as sol–gel synthesis have been explored due to their many advantages over other methods, such as homogeneity, low temperature processing, strong adherence between electrode and electrolyte, etc

[10-12,14]. In the present work, the preparation of La_2NiO_4 via a simpler and environmentally friendly sol-gel route using water as the solvent in the presence of ethanolamine as the directing agent was explored. The effect of the Sr substitution on the A-site on the physical and electrical properties and phase formation of $La_{2-x}Sr_xNiO_4$ ($x = 0$ to 0.8) was also investigated. Data for the samples of the same materials prepared via the solid-state reaction route is also presented for comparison.

4.3 Experimental

4.3.1 Powder Synthesis

For the sol–gel process, the $La_{2-x}Sr_xNiO_4$ powders were prepared by dissolving lanthanum (III) acetate hydrate [$(CH_3COO)_3La•xH_2O$, 99.9%, Sigma–Aldrich}, strontium acetate [$(CH_3COO)_2Sr$, 99.995%, Sigma-Aldrich], and nickel acetate [$(CH_3COO)_2Ni•4H_2O$, 98%, Sigma-Aldrich] in deionized water. The mixture was homogeneously stirred to obtain a clear solution before adding ethanolamine (Labscan Co.), which was used as the directing agent with a 3.21:3 directing agent to cation mole ratio. The mixture was stirred continuously for 6 h before being left at room temperature to gel. The gel was then calcined at 1050°C with a heating rate of 3°C/min for 2 h, resulting in a black powder.

For the solid-state reaction process, the $La_{2-x}Sr_xNiO_4$ powders were prepared by adding the stoichiometric amount of the same starting materials as those used in the sol-gel method into a polypropylene bottle partially filled with 5 mm diameter ZrO_2 balls. The mixture was ball milled at 250 rpm for 10 h. Afterward, the powders were ground and calcined using the same conditions as those prepared via the sol–gel process to obtain the final products.

4.3.2 Characterization

To understand the structure of the synthesized gel formed, a Fourier transform infrared spectroscope (FTIR, Nicolet) was used. The gel obtained from the sol–gel synthesis was directly examined by an FTIR operated at the resolution of 2 cm^{-1} with a scanning range of 400-4000 cm^{-1}. The phase and crystal structures of the calcined samples were characterized using an X-ray diffractometer (XRD, JEOL JDX3530) with a Cu Kα source, 20–80° 2θ range, 0.02° step angle, and 1 s count

time. High resolution XRD scans with 0.003° step angle and 1 s count time using LaB$_6$ (SRM 660a, National Institute of Standards and Technology) as the internal reference standard were performed using a high power XRD (Cu Kα, Rigaku, TTRAX III) on the samples with x = 0, 0.4, and 0.8 to obtain more detailed data on the lattice parameters and unit cell volumes. The morphologies of the powders were investigated using a scanning electron microscope (SEM, JEOL 5200–2AE).

For electrical and CTE measurements, the calcined powders were uniaxially compressed into bars (30 × 5 × 4 mm) at 115 MPa before being sintered in air at 1200°C for 5 h with a heating rate of 5°C/min. The conductivities of the bar specimens were measured as a function of temperature by the standard dc four-terminal method. Four platinum electrode terminals were connected to the sample using a Pt paste (Heraeus). The samples were first heated to 850°C and were stabilized for 2 h in the measurement system. The measurements were performed starting from 850°C to room temperature with 50°C measurement intervals. The cooling rate used was 5°C/min. DCs of 50, 100, 150, 200, and 250 mA were passed through the wires attached to the end of the samples. The corresponding voltages measured between the two inner wires were recorded. The current-voltage responses were linear in all the samples, and the conductivities of the samples were calculated from the specimen dimensions and the slopes of the current-voltage plots obtained. The CTE measurements were carried out from room temperature to 1000°C on a dilatometer (DIL 402 PC. NETZSCH) using 3°C/min heating and cooling rates.

4.4 Results and Discussion

4.4.1 Gel Formation

The formation of three-dimensional La–Sr–Ni network complexes using a simple room-temperature water–based sol-gel process was achieved. Three parameters affecting the sol and gel formation were studied: the molar ratio of water to A-site, directing agent, and gelation time. The amounts of water needed per 1 mol of cation of La$_{2-x}$Sr$_x$NiO$_4$ are as follows: 190, 178, 165, 155, and 145 for x equals to 0, 0.2, 0.4, 0.6, and 0.8, respectively. As the amount of Sr increases, the amount of water needed to dissolve the starting materials decreases by ~25% when adding 0.8

mol Sr as compared to 0 Sr. This is due to the dissolving property of the starting La compound, which has a lower solubility in water compared to the Sr and Ni compounds [15]. Thus, the amount of water needed decreases with decreasing La content. The second processing factor investigated was the choice of directing agent. The mixture solutions formed gel when ethanolamine was introduced, indicating that ethanolamine is an effective agent in controlling hydrolysis and condensation reactions to enhance the formation and stabilization of three-dimensional network structures, as also discovered by Xie *et al.* on the $Sr_{1-x}Ba_xBi_4Ti_4O_{15}$ system [16]. Fig. 4.1 shows the FTIR spectra of the gels produced using ethanolamine. No significant difference was observed between the gels of the different compositions. All spectra show a broad absorption peak ~3360 cm^{-1}, referring to the stretching vibration of hydroxyl groups (O–H) and acetic acid produced during the gel formation. The strong absorption peaks localized at 1550, 1425, and 1380 cm^{-1}, corresponding to the stretching vibration carbonyl groups (COO), were also observed. In this study, ethanolamine can help the gel formation by slowing down the hydrolysis reaction [16]. Thus, the absorption peaks localized at 1014 and 1052 cm^{-1} belong to those of the C–O vibrations. The strong broad peak at 650 cm^{-1} came from the M–O vibrations of the metal–oxygen–metal networks in the gel samples. All samples started to form stable gels after being left at room temperature for 6 h. The gel is stable up to 72 h. Gelation time longer than 72 h resulted in further hydrolysis or reverse reaction (re-esterification) generating excess solvent [17].

4.4.2 Phase Formation

Fig. 4.2 shows the XRD patterns of the $La_{2-x}Sr_xNiO_4$ powders prepared using the different synthesis methods. The La_2NiO_4 phase (JCPDS 34-0314) with the Ruddlesden-Popper structure, K_2NiF_4, was the dominant phase in all cases. The samples prepared by the sol-gel method with a Sr substitution existed as a single phase (Fig. 4.2-1b-e). With no Sr substitution (Fig. 4.2-1a), however, the sample shows extra small peaks at $2\theta = $ 23.544, 26.003, 31.913, 38.678, 42.653, 47.010, 58.037 and 58.463° corresponding to $La_3Ni_2O_7$ (JCPDS 50–0244) and $2\theta = $ 23.387, 25.436, 32.225 and 33.086° corresponding to $LaNiO_3$ (JCPDS 12–0751). From this observation, it is evident that a Sr substitution on the A-site helps stabilize the Ruddlesden-Popper structure. This phenomenon was described by Nei *et al.* who

stated that the formation of $A_{2-x}A_x$ 'BO_4 structure was partially related to the oxidation state of cation at the B–site and that the valence of the B cation was approximately +2 for the K_2NiF_4 structure [18]. This is not always the case as Ni can possess the valences of +2 or +3 in air [19], and therefore, $La_3Ni_2O_7$ (Ni = +2.5)and $LaNiO_3$ phase (Ni = +3) could form. When La^{3+} is substituted by Sr^{2+}, Ni^{3+} could then be compensated by Sr^{2+}. Therefore, it is easier to form the K_2NiF_4 structure when La is partially substituted by Sr. Similar results were found for the samples synthesized via the solid-state method (Fig. 4.2-2d-e) with a small difference in slightly more pronounced additional impurity phases. La_2O_3 (2θ = 29.095, 39.450°, JCPDS 83-1345) and NiO (2θ = 37.249, 43.327°, JCPDS 89-7131) were found in the samples produced via the solid-state synthesis, whereas these phases were almost undetectable in the samples synthesized by the sol-gel method. The difference is likely due to the more intimately mixed starting precursors through the gel formation compared to the solid-state mixing before calcination.

Table 4.1 presents the unit cell parameters and unit cell volumes of the samples with different Sr content. For the samples synthesized either by sol–gel or solid–state methods, the lattice constant (a) decreased quite significantly between x = 0 and x = 0.4. By increasing the amount of Sr doping from x = 0.4 to 0.8, very little change in the lattice constant was observed. The lattice constant along the c–axis, however, increased when x was increased from 0 to 0.4 and decreased again when x = 0.8. The unit cell volume decreases almost linearly with increasing Sr content. These observations are similar to what was reported by Gopalakrishnan et al. [20] The decrease in the overall unit cell volume upon Sr doping, although Sr^{2+} is larger than La^{3+}, could be attributed to the larger effect of the change in ionic radius from the smaller Ni^{2+} to the larger Ni^{3+} with Sr doping.

4.4.3 Morphological Observation

The SEM images of the $La_{2-x}Sr_xNiO_4$ powder after the calcination at 1050°C are shown in Fig. 4.3. For the samples with no Sr substitution, slightly larger particle sizes with higher agglomeration were observed in the case of the solid-state synthesized powder (right), as compared to the powder synthesized via the sol-gel route (left). The substitution of Sr for La had a significant effect on powder morphology. The powder gave a highly agglomerated plate like morphology. No

distinctive particle morphology of the impurity phases could be observed in the SEM images in all samples. Figure 3 also shows the SEM images of the sintered $La_{2-x}Sr_xNiO_4$ fabricated from the powders prepared by the sol-gel and the solid-state methods. For the samples with no Sr substitution, the sample produced from the sol-gel synthesized powder is denser than that produced via the solid-state method. This is expected as the powder from the sol-gel synthesized method had a slightly smaller particle size and to be less agglomerated, and thus should be easier to sinter. Moreover, the lower density of the solid-state materials may be caused by the higher amount of impurities than the sol-gel synthesized materials, as evident in XRD (Fig. 4.2). Such impurity phases could have a pinning effect during sintering. In addition, these impurity phases, La–O and NiO, possess higher melting points than La_2NiO_4 (mp, 1957°C for LaO, 2227°C for NiO, and 1750°C for La_2NiO_4), and thus, a lower sintering rate could be expected for the impure samples compared to the pure samples [21]. This phenomenon is also observed in the lanthanum chromite system by Mori *et al.* [22] and Yang *et al.* [23] who reported that the sintering temperature of materials also depended on the mp of the second phase. The Sr substitution for La on the A-site had a pronounced effect on the morphology of the sintered samples, especially on the sol-gel synthesized samples. Lower density and smaller grain size were observed for the samples with Sr substitution. Reduction in the mobility of the oxygen atoms for $La_{2-x}Sr_xNiO_4$, as compared to La_2NiO_4, was reported by Skinner and Kilner [11]. Therefore, the slower atomic movement could cause a lower sintering rate and result in lower density samples. Another reason for the lower density observation for the samples with Sr substitution may come from the highly agglomerated powder morphology of the starting powders before sintering, as reported in the above section. Highly agglomerated, nonequiaxed particles are expected to yield samples with low green packing density, resulting in final products with low density and high porosity.

4.4.4 Electrical Conductivity

Fig. 4.4 shows the conductivity results of the sintered samples produced by the sol-gel and the solid-state reaction synthesized powders as a function of temperature. In the temperature range (300-900°C) measured, a decrease in conductivity with increasing temperature was observed in all samples, indicating a

metallic conducting behavior of the materials. The result is consistent with what was reported by Ishikawa *et al.* [8] and Goodenough [24] who found that La_2NiO_4 exhibited a semiconducting behavior at temperatures below 300°C and a metallic conducting behavior at temperatures above 300°C. In our study, the conductivity values obtained, as summarized in Table 4.2, were similar to what had been reported by other researchers for the samples with no Sr substitution, having the values between 40 and 100 S/cm in the temperature range of 300–850°C [8-10]. With a small amount of Sr substitution ($x \leq 0.4$), the conductivity decreased and the values increased again at a higher amount of Sr substitution, $x > 0.4$. The results of decreasing conductivity when $x \leq 0.4$ and increasing conductivity when $x > 0.4$ are consistent between the samples synthesized by the solid-state and the sol-gel methods with slightly lower values for the solid-state samples. The slight differences in conductivity values between the sol-gel and the solid-state synthesized samples and the nonsystematic values of the samples with the amount of Sr might be due to the variance in the density of the sintered pellets shown earlier (Fig. 4.3). Nevertheless, it is clearly seen that although the $La_{2-x}Sr_xNiO_4$ samples with $x = 0.8$ show a much more porous structure than the samples with no Sr substitution, the samples still exhibit significantly high conductivities. The conductivity of the $La_{1.2}Sr_{0.8}NiO_4$ sample produced from the sol–gel synthesized powder was much higher, 160 S/cm at 500°C, than those reported by others [8,10] using an even higher amount of Sr.

The Arrhenius plots for electrical conductivity of samples are shown in Fig. 4.5. For the sol-gel samples (Fig. 4.5(a)), the results show the linear relationship in low temperature range (300°C-600°C) with no Sr substitution. When Sr is added ($x = 0.2$), the nearly linear is found with higher temperature range (400°C-850°C). With the higher amount of Sr substitution ($x \geq 0.4$), the linear relationship is found with the whole temperature range (300°C–850°C). The linear relationship agrees with small polaron conduction mechanism which follows the Arrhenius law as shown in Eq.1 where Ea is the activation energy, k is the Boltzmann constant and C is the pre-exponential constant [18,25]. The slight differences between the sol-gel and the solid-state synthesized samples were shown

in Fig. 4.5(b). For the solid-state reaction, the non-linear relationship is found again with the higher amount of Sr substitution ($x \geq 0.8$).

$$\sigma = (\frac{C}{T}) \exp (- \frac{E_a}{kT}) \tag{1}$$

The activation energies with respective temperature ranges are calculated and included in Table 4.3. The results show that the activation energies for the electrical conductivity of $La_{2-x}Sr_xNiO_4$ materials almost follow the Arrhenius law suggesting that the small-polaron hopping conduction mechanism also occurs in $La_{2-x}Sr_xNiO_4$ [26]. In addition, E_a values of all $La_{2-x}Sr_xNiO_4$ compositions are lower than those of the other types of $A_{2-\alpha}A'_\alpha MO_4$ [18, 25] and the perovskite cathode such as $La_{1-x}Sr_xCo_{0.2}Fe_{0.8}O_3$ [26] which could be due to the high carrier concentration in $La_{2-x}Sr_xNiO_4$ [26]. The two different slopes observed in Fig. 4.5 may result from the tetragonal-orthorhombic phase transition which general found in these materials [27]. This could be due to Sr helps stabilized the $La_{2-x}Sr_xNiO_4$ structures and might cause no phase transition. It is seen that the two different slopes disappear with Sr content increase and indicate that the small polaron conduction can occur with higher temperatures. However, E_a values are in agreement with the trend of electrical conductivity which increases with Sr content up to 0.4–0.6 mol ratio and then decrease as Sr content up to 0.8 mol ratio.

4.4.5 Thermal Expansion

Fig. 4.6 shows the expansion rates of $La_{2-x}Sr_xNiO_4$ prepared via the sol-gel process when x is 0 (____), 0.4 (......), and 0.8 (___.) and prepared by the solid-state reaction when x is 0 (_ _ _), 0.4 (___. .), and 0.8 (- - - -). With no Sr substitution ($x = 0$), a nonlinear expansion rate at low (150-300°C) and high (more than 800°C) temperatures was observed. The reason for this behavior may be similar to what was reported by Skinner and Kang for $CeNbO_{4+\delta}$ compound, which have been demonstrated to contain mobile oxygen interstitials [28]. The change at low temperature was attributed to the oxidation of the stoichiometric compound, whereas the change at high temperature is still unclear. The expansion rate with temperature is not clearly observed for the Sr substituted compound, however. This might be due to the addition of Sr to help stabilize the A_2BO_4 structure, as shown earlier by the

XRD results. The TEC values of the Sr-substituted compounds from Fig. 4.6 are listed in Table 4.2, and are in the range of 12.4-13.6 × $10^{-6\circ}C^{-1}$. As can be seen, the values are much closer to those commonly used for IT-SOFC electrolytes such as Ceria Gadolinium Oxides (CGO) (13.6 × $10^{-6\circ}C^{-1}$) than some of the cathode material candidates such as $La_{0.3}Sr_{0.7}CoO_{3-x}$ (TEC = 25.0 × $10^{-6\circ}C^{-1}$) and $La_{0.6}Sr_{0.4}Fe_{0.2}Co_{0.8}O_3$ (TEC = 21.4 × $10^{-6\circ}C^{-1}$) [29]. Also, the samples from the sol-gel process provide a lower expansion than those from the solid-state reaction because of the smaller and more homogeneous pore size of the sol–gel samples, as shown in the SEM micrographs (Fig. 4.3). No systematic relation between the amount of Sr and the thermal expansion coefficient (TEC) values could be observed, however. This is likely due to the difference in density of the sintered samples.

4.5 Conclusions

The synthesis of $La_{2-x}Sr_xNiO_4$ (x = 0, 0.4, and 0.8) via a simple room-temperature sol-gel process using a water-based solvent in presence of a little amount of ethanolamine was successfully carried out. Suitable gelation time was in the range of 6-72 h. depending on the amount of Sr added. The sol-gel method was shown to yield more homogenous powders with higher purity than the solid-state reaction method. The substitution of Sr for La on the A-site affected the phase. sintering, and conducting behavior of the synthesized samples. The $La_{2-x}Sr_xNiO_4$ phase was more stable than La_2NiO_4, resulting in only single phase. The TEC values of the materials were close to and should be suitably close to those of IT-SOFC electrolytes. A high conductivity $La_{1.2}Sr_{0.8}NiO_4$ cathode, 160 S/cm at 500°C, was obtained via the sol-gel powder.

4.6 Acknowledgements

4.7 References

[1] Ralph, J. M., Schoeler, A. C., and Krumpelt, M. (2001) Materials for lower temperature solid oxide fuel cells. J. Mater. Sci., 36, 1161-1172.

[2] Jiang, S. P. (2002) A Comparison of O_2 reactions on porous (La,Sr)MnO_3 and (La,Sr)(Co,Fe)O_3 electrodes. Solid State Ionics, 146, 1-22.

[3] Qiu, L., Ichikawa, T., Hirano, A., Imanishi, N., and Takeda, Y. (2003) $Ln_{1-x}Sr_xCo_{1-y}Fe_yO_{3-\delta}$ (Ln = Pr, Nd, Gd; x = 0.2, 0.3) for the electrodes of solid oxide fuel cells. Solid State Ionics, 158, 55-65.

[4] Amow, G. and Skinner, S. J. (2006) Recent developments in Ruddlesden-Popper nickelate systems for solid oxide fuel cell cathodes. J. Solid State Electrochem., 10, 538-546.

[5] Fontaine, M. L., Laberty-Robert, C., Ansart, F., and Tailhades, P. (2006) Composition and porosity graded $La_{2-x}NiO_{4+\delta}$ ($x\geq0$) interlayers for SOFC: Control of the microstructure via a sol-gel Process. J. Power Source, 156, 33-38.

[6] Chiba, R., Yoshimura, F., and Sakurai, Y. (1999) An investigation of $LaNi_{1-x}Fe_xO_3$ as a cathode material for solid oxide fuel cells. Solid State Ionics, 124, 281-288.

[7] Kharton, V.V., Tsipis, E.V., Yaremchenko, A.A., and Frade, J.R. (2004) Surface-limited oxygen transport and electrode properties of $La_2Ni_{0.8}Cu_{0.2}O_{4+\delta}$. Solid State Ionics, 166, 327-337.

[8] Ishikawa, K., Kondo, S., Okano, H., Suzuki, S., and Suzuki, Y. (1987) Nonstoichiometry and electrical resistivity in two mixed metal oxides, La_2NiO_{4-x} and $LaSrNiO_{4-x}$. Bull. Chem. Soc. Jpn., 60, 1295-1298.

[9] Aguadero, A., Escudero, M. J., Pérez, M., Alonso, J. A., and Daza, L. (2007) Hyperstoichiometric $La_{1.9}Sr_{0.1}NiO_{4+\delta}$ mixed conductor as novel cathode for intermediate temperature solid oxide fuel cells. J. Fuel Cell Sci.Tech., 4, 294-298.

[10] Makhnach, L.V., Pankov, V.V., and Strobel, P. (2008) High–temperature oxygen non-stoichiometry, conductivity and structure in strontium–rich nickelates $La_{2-x}Sr_xNiO_{4-\delta}$ (x = 1 and 1.4). Mater. Chem. Phys., 111, 125-130.

[11] Skinner, S. J. and Kilner, J.A. (2000) Oxygen diffusion and surface exchange in $La_{2-x}Sr_xNiO_{4+\delta}$. Solid State Ionics, 135, 709-712.

[12] Fontaine, M.L., Laberty-Robert, C., Verelst, M., Pielaszeck, J., Lenormand, P., Ansart, F., and Tailhades, P. (2006) Synthesis of $La_2NiO_{4+\delta}$ Oxides by sol–gel process: structural and microstructural evolution from Amorphous to nanocrystallized powders. Mater. Res. Bull., 41, 1747-1753.

[13] Bevilacqua, C. M., Montini, T., Tavagnacco, C., Vicario, G., Fornasiero, P., and Graziani, M. (2006) Influence of synthesis route on morphology and electrical properties of $LaNi_{0.6}Fe_{0.4}O_3$. Solid State Ionics, 177, 2957-2965.

[14] Bilger, S., Syskakis, E., Naoumidis, A., and Nickel, H. (1992) Sol-gel synthesis of strontium-doped lanthanum manganite. J. Am. Ceram. Soc., 75(4), 964-970.

[15] Stephen, H. (1963) Solubilities of Inorganic and Organic Compounds. (pp 312-728). Pergamon, Oxford.

[16] Xie, D., Pan, W., and Shi, H. (2003) Synthesis and characterization of $Sr_{1-x}Ba_xBi_4Ti_4O_{15}$ ferroelectric materials. Mater. Sci. Eng., B99, 352-355.

[17] Brinker, C. J. and Scherer, G. W. (1990). Sol-Gel Science: The Physics and Chemistry of Sol-Gel Processing. (pp 358-364). Academic Press, San Diego.

[18] Nie, H.W., Wen, T.-L., Wang, S.R., Wang, Y.S., Guth, U., and Vashook, V. (2006) Preparation, thermal expansion, chemical compatibility, electrical conductivity and polarization of $A_{2-\alpha}A'_\alpha MO_4$ (A=Pr, Sm; A'=Sr; M=Mn, Ni; α=0.3, 0.6) as a new cathode for SOFC. Solid State Ionics, 177, 1929-1932.

[19] Amow, G. and Davidson, I.J. (2005). Preliminary investigation of the higher–order Ruddlesden-Popper phases for IT-SOFC cathodes, $La_{n+1}Ni_nO_{3n+1}$ (n = 2 and 3). Paper presented at Solid Oxide Fuel Cells IX (SOFC-IX), Volume 2 Materials (pp 1745-1750). Electrochemical Society, New Jersey, USA.

[20] Gopalakrishnan, J., Colsmann, G., and Reuter, B. (1977) Studies on the $La_{2-x}Sr_xNiO_4$ ($0 \le x \le 1$) system. J. Solid State Chem., 22, 145-149.

[21] Zinkevich, M. and Aldinger, F. (2004) Thermodynamic analysis of the ternary La–Ni–O system. J. Alloys Compd., 375, 147-161.

[22] Mori, M., Hiei, Y., and Sammes. N. M. (2006) Sintering behavior of Ca– or Sr–doped $LaCrO_3$ perovskites including second phase of $AECrO_4$ (AE = Sr, Ca) in air. Solid State Ionics, 135, 743-748.

[23] Yang, Y. J., Wen, T. L., Tu, H., Wang, D. Q., and Yang, J. (2000) Characteristics of lanthanum strontium chromite prepared by glycine nitrate process. Solid State Ionics, 135, 475-479.

[24] Goodenough, J. B. (1973) Interpretation of the transport properties of $Ln_2 NiO_4$ and Ln_2CuO_4 compounds. Mat. Res. Bull., 8, 423-432.

[25] Shen, Y., Zhao, H., Liu, X., and Xu, N. (2010) Preparation and electrical properties of Ca-doped $La_2NiO_{4+\delta}$ cathode materials for IT-SOFC. Phys. Chem. Chem. Phys., 12, 15124-15131.

[26] Tai, L.-W., Nasrallah, M.M., Anderson, H.U., Sparlin, D.M., and Sehlin, S.R. (1995) Structure and electrical properties of $La_{1-x}Sr_xCo_{1-y}Fe_yO_3$. Part 2. The system $La_{1-x}Sr_xCo_{0.2}Fe_{0.8}O_3$. Solid State Ionics, 76, 273-283.

[27] Aguadero, A., Escudero, M. J., Perez, M., Alonso, J. A., Pomjakushin, V., and Daza, L. (2006) Effect of Sr content on the crystal structure and electrical properties of the system $La_{2-x}Sr_xNiO_{4+\delta}$ ($0 \le x \le 1$). Dalton Trans., 4377-4383.

[28] Skinner, S. J. and Kang, Y. (2003) X–Ray Diffraction studies and phase transformations of $CeNbO_{4+\delta}$ using in situ techniques. Solid State Sci., 5, 1475-1479.

[29] Ullmann, H., Trofimenko, N., Tietz, F., Stöver, D., and Ahmad-Khanlou, A. (2000) Correlation between thermal expansion and oxide ion transport in mixedc Perovskite-type oxides for SOFC cathodes. Solid State Ionics, 138, 79-90.

Table 4.1 Unit cell dimensions and unit cell volumes of $La_{2-x}Sr_xNiO_4$ synthesized via sol-gel and solid state methods

Parameter	$La_{2-x}Sr_xNiO_4$					
	Sol-gel			Solid state		
	$x = 0$	$x = 0.4$	$x = 0.8$	$x = 0$	$x = 0.4$	$x = 0.8$
a (Å)	4.0206	3.9768	3.9753	4.0135	3.9754	3.9768
c (Å)	13.072	13.084	12.960	13.040	13.080	12.956
V (Å³)	211.31	206.96	204.81	210.05	206.71	204.89

Table 4.2 Electrical conductivities and TEC of samples produced via the different synthesis routes

$La_{2-}Sr_xNiO_4$	Sol-gel		Solid state	
	*TEC × 10⁻⁶ ($°C^{-1}$)	**σ (S/cm)	*TEC × 10⁻⁶ ($°C^{-1}$)	**σ (S/cm)
x = 0	13.1	50	13.2	50
x = 0.2	-	40	-	34
x = 0.4	13.1	38	13.6	27
x = 0.6	-	96	-	82
x = 0.8	12.4	160	12.8	90

* The thermal expansion coefficient measured at 400-700°C.
** The electrical conductivity measured at 500°C.

Table 4.3 Activation energy with respective temperature ranges for the electrical conductivity for the different materials

Sr content, x (mol ratio)	$La_{2-x}Sr_xNiO_{4+\delta}$				$La_{2-x}Ca_xNiO_{4+\delta}$ [25]		$A_{2-a}A'_aMO_4$ [18]						$La_{1-x}Sr_xCo_{0.2}Fe_{0.8}O_3$ [26]	
	Sol-Gel		Solid State				$Sm_{1.4}Sr_{0.6}NiO_4$		$Pr_{1.4}Sr_{0.6}NiO_4$		$Pr_{1.7}Sr_{0.3}NiO_4$			
	Temp (°C)	Ea (eV)	Temp (°C)	Ea (eV)	Temp (°C)	Ea (eV)	Temp (°C)	Ea (eV)	Temp (°C)	Ea (eV)	Temp (°C)	Ea (eV)	Temp (°C)	Ea (eV)
x = 0.0	300-600	0.016	300-600	0.020	100-550	0.055	100-900	0.1226	100-900	0.067	100-900	0.091	100-400	0.62
	-	-	-	-	-	-							500-900	0.32
x = 0.1	-	-	-	-	100-600	0.052							400-900	0.18
x = 0.2	300-400	0.029	300-400	0.029	100-600	0.055							200-800	0.14
	400-850	0.020	400-850	0.017	-	-							-	-
x = 0.3	-	-	-	-	100-600	0.061							100-600	0.13
x = 0.4	300-850	0.035	400-850	0.034	-	-							100-500	0.10
x = 0.6	300-850	0.036	400-850	0.022	-	-							-	-
x = 0.8	300-850	0.020	300-400	0.040	-	-							-	-
	-	-	400-850	0.013	-	-							-	-

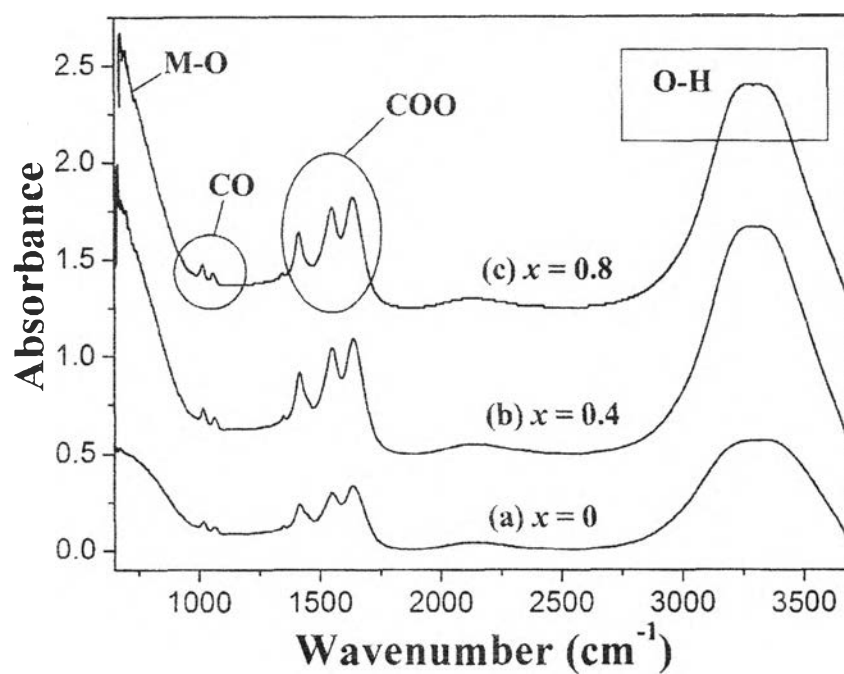**Figure 4.1** FTIR spectra of the dried gels of $La_{2-x}Sr_xNiO_4$ prepared using ethanolamine for (a) $x = 0$, (b) $x = 0.4$, and (c) $x = 0.8$.
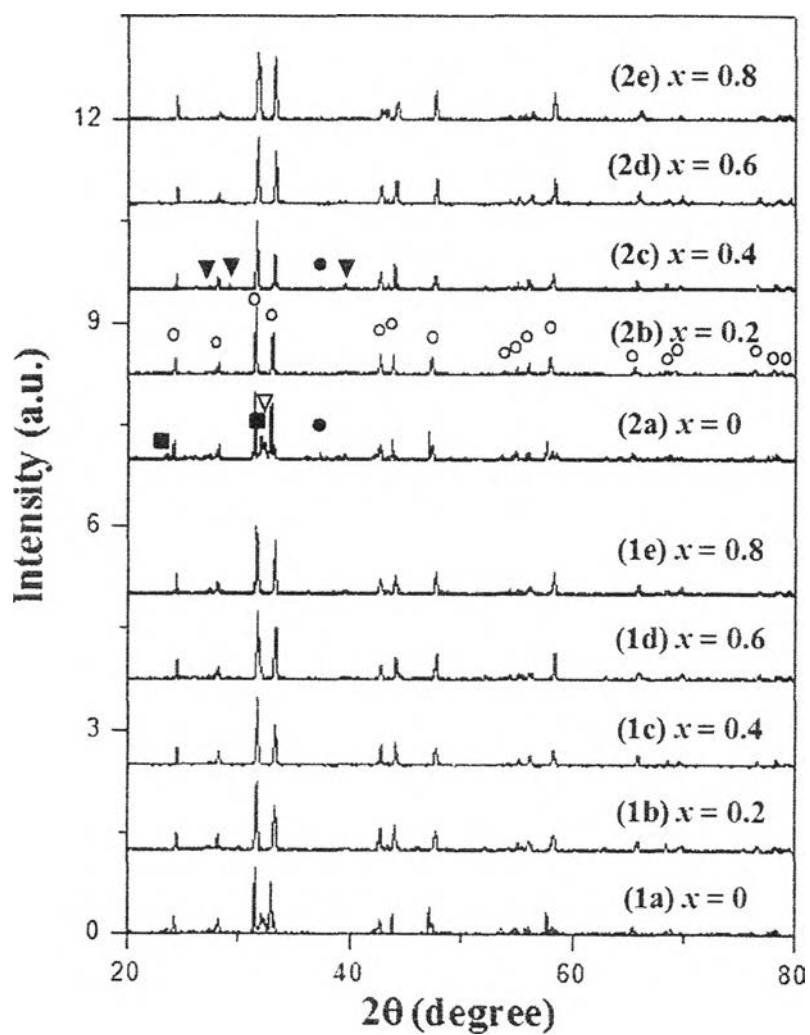
Figure 4.2 XRD patterns of the calcined $La_{2-x}Sr_xNiO_4$ powders prepared via the sol-gel and the solid state reaction processes when x is 1a-e and 2a-e, respectively ($\circ$ La_2NiO_4, ■ $La_3Ni_2O_7$, ∇ $LaNiO_3$, ● La_2O_3 and ▼ NiO).

Sol–gel   **Solid–state**

Powder   Sintered   Powder   Sintered
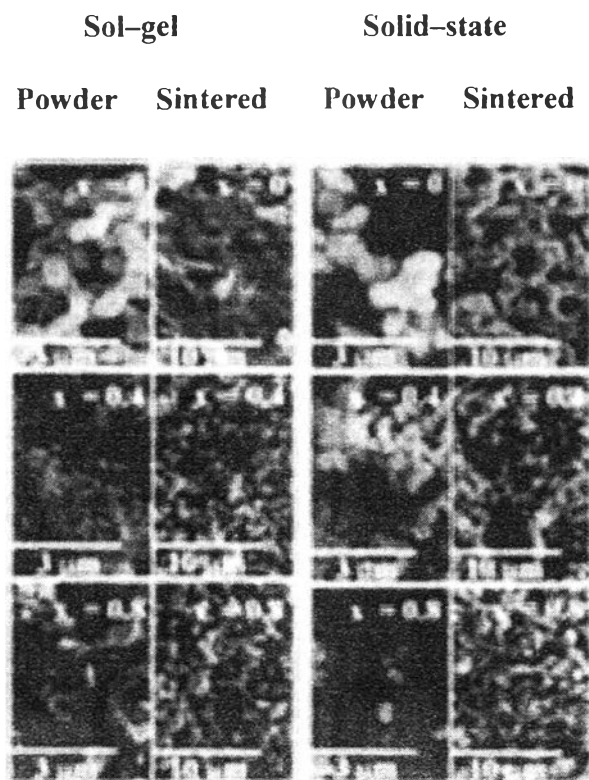
Figure 4.3   SEM images of $La_{2-x}Sr_xNiO_4$ powder calcined at 1050°C and the samples sintered at 1200°C prepared by the sol-gel (left) and the solid state (right) methods.
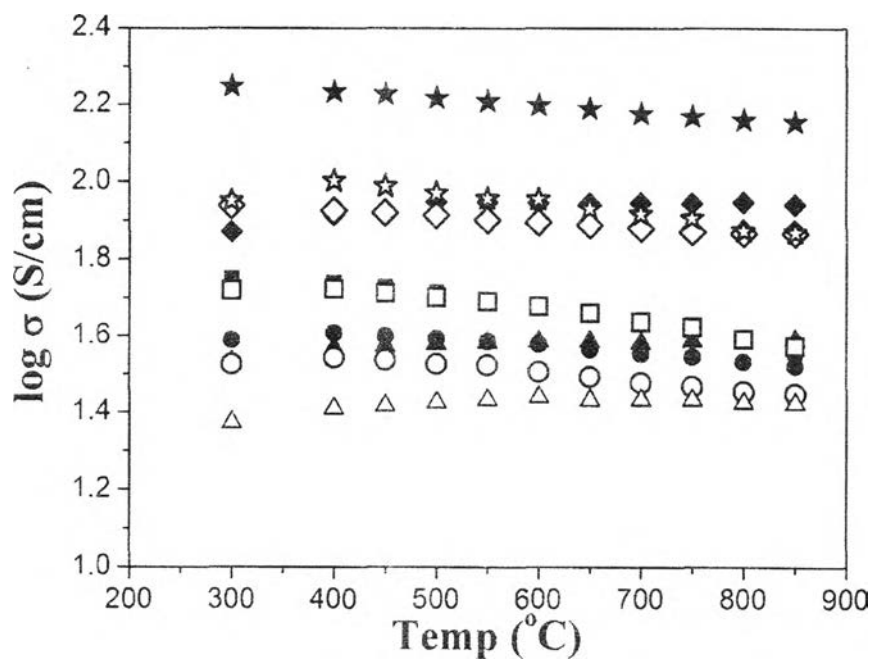
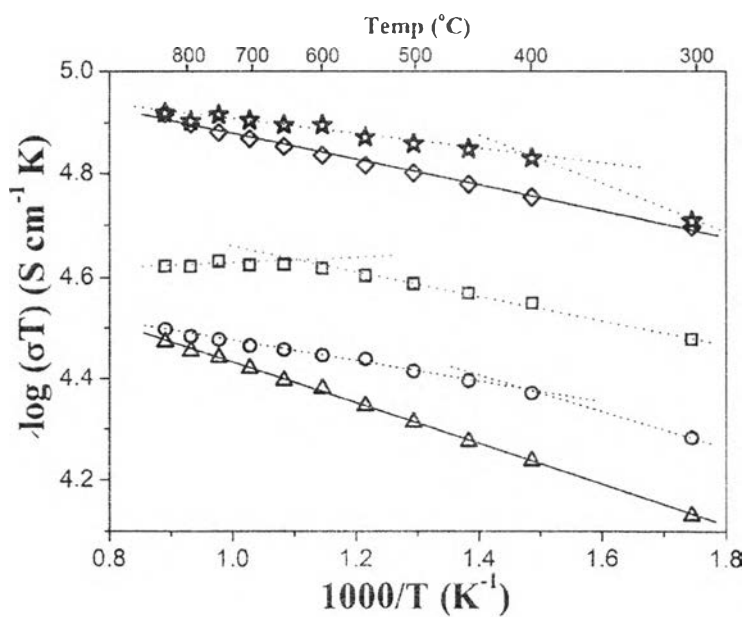**Figure 4.4** Electrical conductivity vs temperature plot of $La_{2-x}Sr_xNiO_4$ prepared via the sol-gel process (closed symbols) when x is 0 (■), 0.2 (●), 0.4 (▲), 0.6 (◆), and 0.8 (★) and $La_{2-x}Sr_xNiO_4$ prepared by the solid state reaction (opened symbols) when x is 0 (□), 0.2 (○), 0.4 (△), 0.6 (◇) and 0.8 (☆).

Temp (°C)

(a)

Temp (°C)

(b)
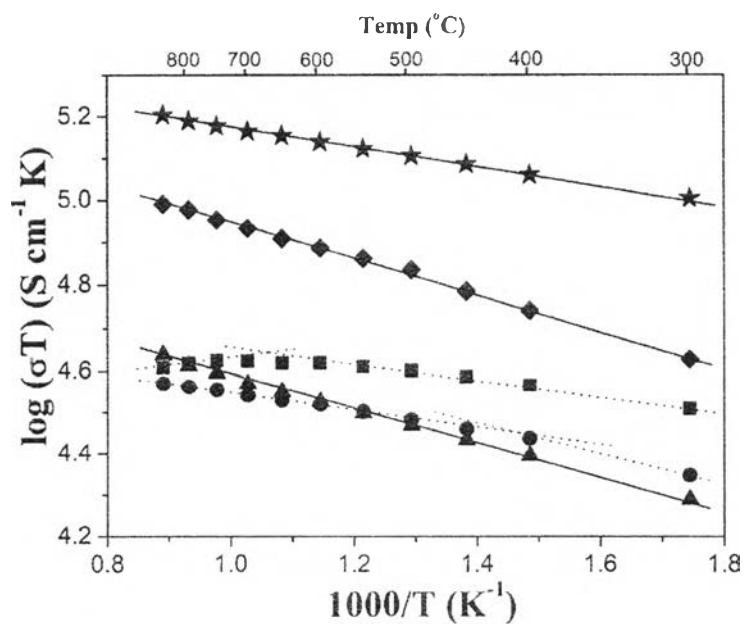
Figure 4.4 Log σT versus 1000/T in air of La$_{2-x}$Sr$_x$NiO$_4$ prepared via (a) the sol-gel process (closed symbols) when x is 0 (····■····), 0.2 (····●····), 0.4 (—▲—), 0.6 (—◆—), and 0.8 (—★—) and La$_{2-x}$Sr$_x$NiO$_4$ prepared by (b) the solid state reaction (opened symbols) when x is 0 (····□····), 0.2 (····○····), 0.4 (····△····), 0.6 (—◇—) and 0.8 (—☆—).

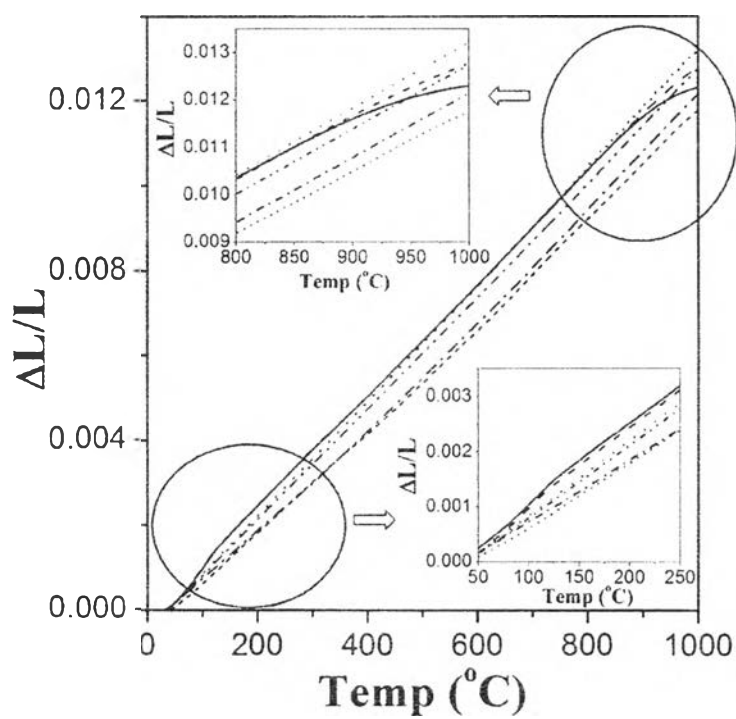**Figure 4.6** Expansion rates of La$_{2-x}$Sr$_x$NiO$_4$ prepared via the sol-gel process when x is 0 (___), 0.4 (......), and 0.8 (__.) and La$_{2-x}$Sr$_x$NiO$_4$ prepared by the solid state reaction when x is 0 (_ _ _), 0.4 (__ . .), and 0.8 (- - - -).